Kinetic modeling of the first step of Mn_2O_3/MnO thermochemical cycle for solar hydrogen production

J.A. Botas[1], J. Marugán[2,*], R. Molina[2], C. Herradón[1]

[1] *Department of Chemical and Energy Technology, Rey Juan Carlos University, c/ Tulipán, s/n, 28933, Móstoles, Spain*

[2] *Department of Chemical and Environmental Technology, Rey Juan Carlos University, c/ Tulipán, s/n, 28933, Móstoles, Spain.*

(*) corresponding author: Tel.: +34 91 664 7466; fax: +34 91 488 7068; E-mail address: javier.marugan@urjc.es

Published on

International Journal of Hydrogen Energy 37 (2012) 18661–18671.

doi:10.1016/j.ijhydene.2012.09.114

Abstract

This work reports the kinetic study of the first step of the Mn_2O_3/MnO thermochemical cycle for hydrogen production by water splitting. The reaction kinetics of Mn (III) oxide thermal reduction has been evaluated using dynamic thermogravimetric analysis at constant heating rate under nitrogen flow. This way the reaction rate can be described as a function of temperature and different kinetic models were fitted to the experimental data obtained from thermogravimetric experiments. A good fitting can be observed for each experiment, although a significant disparity in the values estimated for the Arrhenius parameters has been found (activation energies and pre-exponential factors). Unique values for the kinetic parameters have been calculated by application of a multivariate non-linear regression method for the simultaneous fitting of data from all the experiments carried out at different heating ramps. However, also in this case the values of the Arrhenius parameters are significantly different depending on the chosen kinetic equation. Optimal kinetic parameters have been finally calculated through the estimation of activation energy values by model-free isoconversional methods and using a rigorous multivariate nonlinear regression for the calculation of the model-dependant pre-exponential factors.

Keywords: Thermochemical water splitting, Hydrogen production, Manganese oxide, Kinetic modeling

Introduction

Currently most of the energy production in the world comes from fossil fuels. However, increasingly ambitious policy targets to reduce greenhouse gases emissions as well as the need of sustainable energy systems have made of hydrogen a promising energy carrier for a future low carbon energy economy [1]. Of course, a massive hydrogen use is reasonable only if renewable energy sources are used for its production. In this context, water splitting by solar-driven thermochemical cycles represents a promising technology for this purpose [2].

Current research efforts have been focused mainly on thermochemical cycles based on iron or zinc oxides. They consist of two chemical reactions where the metal oxide is first thermally reduced and then oxidized with water, being the overall reaction the splitting of water in ½ mol of O_2 per mol of H_2. Despite their apparent simplicity, there are difficulties associated to the high temperatures required (between 1920 ºC and 2230 ºC) and the attention has diverted to thermochemical cycles based on more than two steps, which require lower temperatures. Consequently, alternative cycles such as the Mn-oxide cycle have been proposed [3].

The cycle Mn_2O_3/MnO consists of three steps,

$$1/2\ Mn_2O_3 \rightarrow MnO + 1/4\ O_2 \quad \text{(R1)}$$

$$MnO + NaOH \rightarrow NaMnO_2 + 1/2\ H_2 \quad \text{(R2)}$$

$$NaMnO_2 + 1/2\ H_2O \rightarrow 1/2\ Mn_2O_3 + NaOH \quad \text{(R3)}$$

The thermal reduction of Mn(III) oxide (R1) to the lower-valence Mn(II) oxide (MnO) is an endothermic step and theoretically requires temperatures above 1560 ºC [3], what makes it compatible with concentrated solar irradiation. This thermal reduction of Mn_2O_3 into MnO occurs through two sequential reaction steps:

$$Mn_2O_3 \rightarrow 2/3\ Mn_3O_4 + 1/6\ O_2 \quad \text{(R4)}$$

$$2/3\ Mn_3O_4 \rightarrow 2\ MnO + 1/3\ O_2 \quad \text{(R5)}$$

Little work can be found in literature regarding to this reduction step of the Mn-oxide thermochemical cycle for water splitting and it is mainly focused on theoretical and thermodynamic studies [3]. However, understanding of the reduction step is critical for evaluating the overall efficiency of the process, as the feasibility of the cycle depends on the high conversion of the Mn_2O_3 to MnO [3]. A recent work by Francis et al. [4] has reported the thermal reduction of manganese oxide in a high temperature aerosol reactor (AFR), including the determination of rate constants considering the Avrami–Erofeev nucleation and growth mechanism to derive the kinetic expressions. This is a common approach found in the literature to obtained kinetic parameters by direct regression of experimental data to previously defined kinetic expressions with different mechanistic basis, choosing the model that leads to the best fitting. The main disadvantage of this technique is that the values of the kinetic parameters can be strongly dependent on the chosen model, even for similar regression statistics.

In the present work, different numerical and modeling approaches have been evaluated for the determination of the kinetic parameters of the reactions involved in the first step of the Mn_2O_3/MnO thermochemical cycle for H_2 production by water splitting. Kinetic studies are usually carried out under both isothermal and non-isothermal heating conditions [5]. However, due to the high temperatures in which the reactions take place, it is hardly difficult to conduct isothermal experiments, as the reaction starts before reaching the desired temperature even for high heating rates. Thus, a non-isothermal approach at different heating rates has been used to include in the kinetic model the unavoidable evolution of the temperature during the process.

2. Experimental

The thermal reduction of commercial Mn_2O_3 (Sigma-Aldrich) has been studied by thermogravimetric analysis (TGA) using a TGA/DSC1 STAR^e System (Mettler Toledo). A scheme of the equipment is shown in Figure 1. The experiments were carried out under nitrogen flow (80 mL/min), to keep an inert environment around the Mn-oxide solid sample (50 mg) placed in a Pt90/Rh10 crucible over a sapphire disc to avoid direct contact with the

thermobalance support. Preliminary experiments were conducted to verify the inert behaviour of the crucible in the whole range of temperatures used in this study. The gas flow rate value was previously optimized by increasing the gas flow until reaching constant weight loss profiles to guarantee that the experimental results are not controlled by external mass transport.

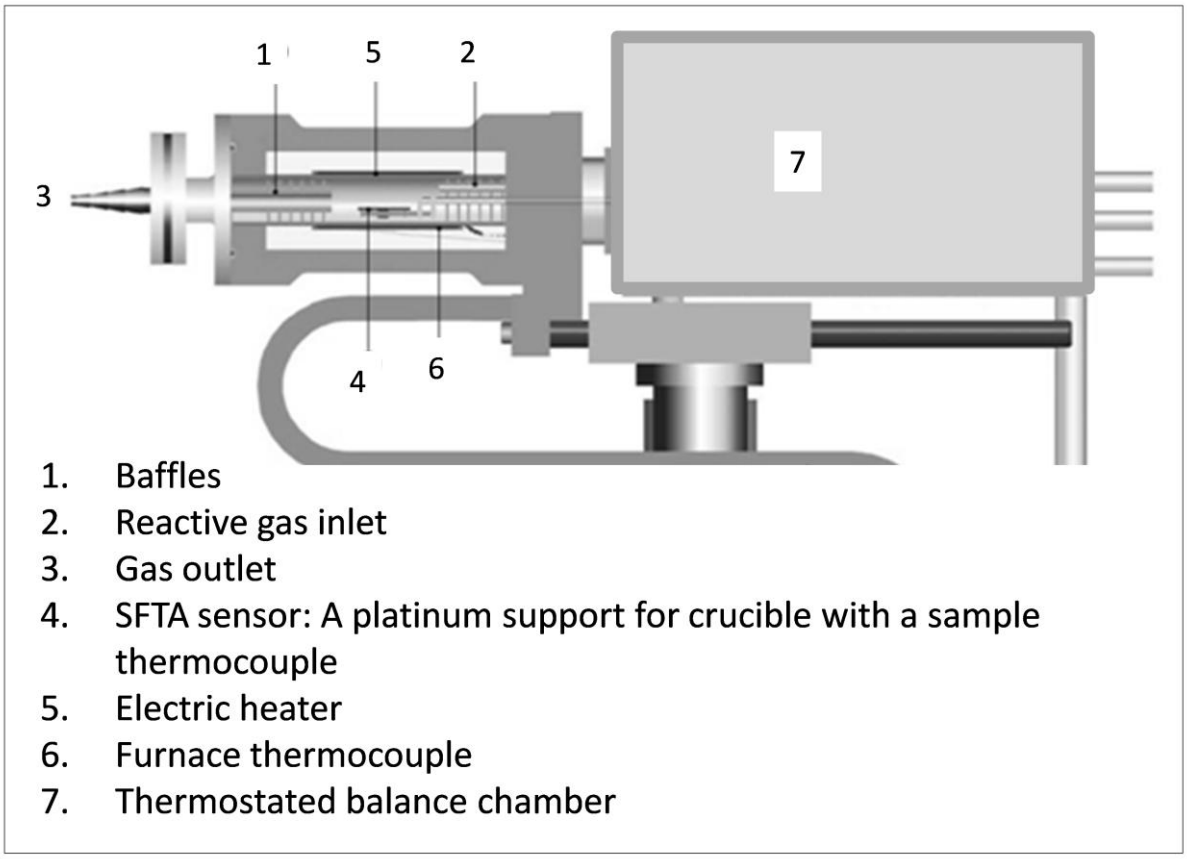

Figure 1. Scheme of the thermogravimetric device (based on the TGA/DSC 1 Product Brochure document from Mettler Toledo webpage, http://es.mt.com).

The temperature programme starts from room temperature with a heating rate of 20 °C/min up to 150 °C. This temperature was kept constant for 30 minutes to remove water traces in the solid sample. Then, the temperature was risen up to 1500 ºC with different heating rates of 2, 5, 10 and 20 °C/min. Finally, the sample was cooled down to 40 °C with a rate of 10 °C/min. As the reduction process takes place at temperatures above 500 ºC, the relative weight loss experimental curves have been corrected assuming the weight at 500 ºC as the initial value in order to avoid distorsions due to low temperature drying processes. Under these experimental conditions normalised TGA data can be used to calculate the kinetics of both reactions, taking

into account that the weight loss along the process is directly related to the release of oxygen following reactions R4 and R5. Normalised TGA curves have been determined by calculation the reaction conversion as the ratio between the experimental weight loss and the maximum weight loss of the step, estimated theoretically from the reaction stoichiometry.

3. Results and discussion

3.1. Experimental TGA results

Figure 2 shows the experimental weight loss curves obtained in TGA experiments at four different heating rates. Both reactions steps R4 and R5 can be clearly distinguished, taking place sequentially in the range 600 to 900 ºC and above 1200 ºC, respectively. Theoretical weight loss for total conversion of Mn_2O_3 to Mn_3O_4 according to the stoichiometry of reaction R4 is 3.4 %, which is achieved under the four heating rates. Total conversion of Mn_3O_4 to MnO according to the reaction R5 would correspond to an additional weight loss of 6.8 %, which would be obtained at temperatures above 1500ºC, the operational limit of the TGA equipment employed in this work, or for longer reaction time under isothermal conditions. As it can be noticed, the lower heating rate the higher reaction conversion, as a consequence of the longer reaction time. Reactions R4 and R5 have been studied independently, using data from 500 ºC to 1100 ºC for reaction R4 and data from 1100 to 1500 ºC for reaction R5.

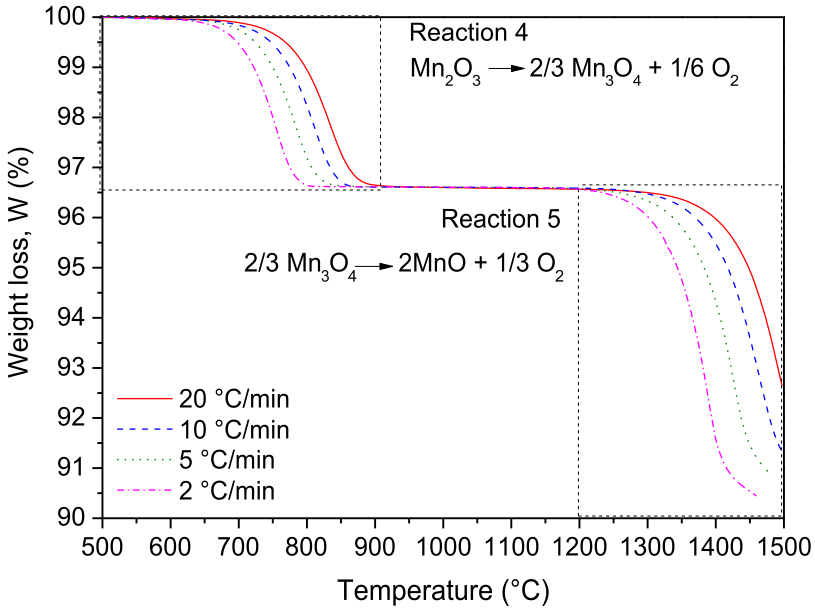

Figure 2. TGA experimental weight loss profiles obtained from the thermal reduction of Mn_2O_3 at different heating rates.

3.2. Kinetic modeling

The basic kinetic equation of non-isothermal techniques is adapted from the isothermal formalism expressed in Eq.1:

$$\frac{d\alpha}{dt} = k(T) f(\alpha) \qquad \text{(Eq.1)}$$

where α is the conversion, T the temperature, $k(T)$ the temperature dependant rate constant (kinetic constant) and $f(\alpha)$ the reaction model that describes the dependence of the reaction rate on the conversion. The temperature dependence of k can be described by the Arrhenius equation, leading to Eq.2:

$$\frac{d\alpha}{dt} = A exp\left(\frac{-E}{RT}\right) f(\alpha) \qquad \text{(Eq.2)}$$

in which E is the activation energy and A the pre-exponential factor. In case of non-isothermal conditions at constant heating rate ($\beta = dT/dt$), the time dependence of the above equations can be eliminated (Eq.3).

$$\frac{d\alpha}{dT} = \frac{d\alpha}{dt}\frac{dt}{dT} = \frac{A}{\beta} exp\left(\frac{-E}{RT}\right) f(\alpha) \qquad \text{(Eq.3)}$$

3.2.1. Model fitting methods

The differential equation Eq.3 can be solved by selecting a specific kinetic model for the function $f(\alpha)$ [6]. The estimation of the kinetic parameters for each model can be carried out by fitting the equation to the experimental data using a nonlinear regression method coupled with a numerical integration procedure for the resolution of the differential equations [7]. Application of this method to solid-state reactions has been criticized due to the assumption of

irreversible reaction and because the influence of mass transfer is neglected. Considering that reactions R4 and R5 can be formulated as specific cases of the following general reaction [8]:

$$\mathrm{A\ (solid)} \rightarrow \mathrm{B\ (solid)} + \mathrm{C\ (gas)} \qquad \text{(R6)}$$

the hypothesis of irreversible reactions is usually based on the use of a gas flow high enough to assume a negligible partial pressure of C component.

On the other hand, solid-state processes obviously include sequential elementary steps of mass transport and chemical reaction with different activation energies and contributions to the overall reaction rate. Consequently, the calculated kinetic parameters must be considered as apparent values of the global process [9]. In a first approach, experimental TGA curves were individually fitted to the different kinetic model equations for solid-state reactions cited in Table 1. Those equations were selected from a complete list of 26 kinetic models for solid-state reactions found in literature [6]. The selection was made according to the shape of the theoretical α *vs.* T profiles corresponding to each model [9]. As both reactions take place sequentially, they have been fitted independently (the kinetic equation should not be necessary the same in both cases) following the normalization of the conversion, α, of each individual step R4 and R5 (normalized conversion data for each reaction are shown in Figure 3). Thus, those models with theoretical curve's shape different from those shown in Figure 3 were discarded.

Table 1. Kinetic models for solid state reactions.

Kinetic Model		Kinetic mechanism	$f(\alpha)$
Kinetic-order models	**F_0**	Zero-order	1
	F_1	First-order	$1-\alpha$
	$F_{1.5}$	One and a half order	$2\cdot(1-\alpha)^{1.5}$
	F_2	Second order	$(1-\alpha)^2$
	F_3	Third order	$0.5\cdot(1-\alpha)^3$
Nucleation models	**A_2**	Avrami-Erofeev	$2\cdot(1-\alpha)\cdot(-\log(1-\alpha))^{0.5}$
	A_3	Avrami-Erofeev	$3\cdot(1-\alpha)\cdot(-\log(1-\alpha))^{2/3}$
	A_4	Avrami-Erofeev	$4\cdot(1-\alpha)\cdot(-\log(1-\alpha))^{3/4}$
	P_2	Power law	$2\cdot\alpha^{0.5}$
	P_3	Power law	$3\cdot\alpha^{2/3}$
	P_4	Power law	$4\cdot\alpha^{3/4}$
Contraction models	**R_2**	Contracting cylinder model	$2\cdot(1-\alpha)^{0.5}$
	R_3	Contracting sphere model	$3\cdot(1-\alpha)^{2/3}$
Diffusion models	**D_1**	Parabola law (1-D diffusion)	$(2\cdot\alpha)^{-1}$
	D_2	Valensi equation (2-D diffusion)	$(-\log(1-\alpha))^{-1}$
	D_3	Jander equation (3-D diffusion)	$(3/2)\cdot(1-\alpha)^{2/3}\cdot[1-(1-\alpha)^{1/3}]$
	D_4	Ginstling-Brounshtein equation	$(3/2)\cdot[(1-\alpha)^{-1/3}-1]$
	D_5	Zhuravlev, Lesokin and Tempelman equation	$(3/2)\cdot(1-\alpha)^{4/3}\cdot[(1-\alpha)^{-1/3}-1]$
	D_6	Anti-Jander equation	$(3/2)\cdot(1+\alpha)^{2/3}\cdot[(1+\alpha)^{-1/3}-1]$

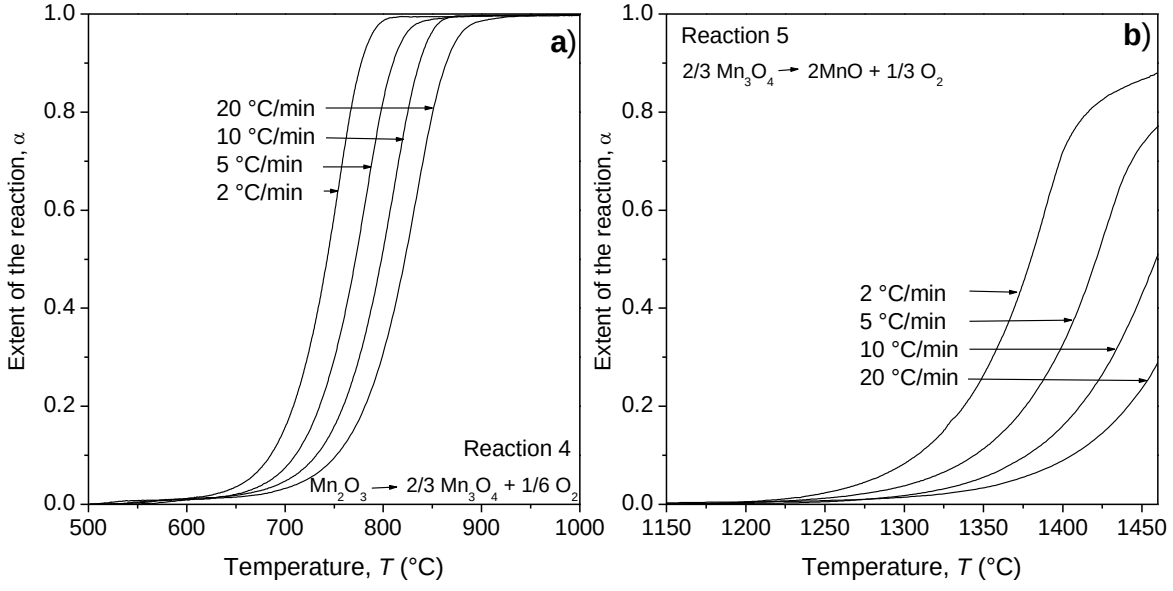

Figure 3. Normalized TGA experimental data obtained for: a) reaction R4, and b) reaction R5.

Direct model fitting were carried out by formulation of a nonlinear programming problem that minimize the sum of quadratic residuals (SQR) using a sequential quadratic programming (SQP) method. The objetive function is coupled with a fourth-order Runge-Kutta method for the resolution of the differential equation Eq.3 assuming each specific kinetic equation. Table 2 summarizes the results of the three models that best fit the experimental data, whereas Figure 4 shows the good agreement between the calculated data and the experimental results.

Table 2. Kinetic parameters calculated for the best individual fitting of the experimental TGA curves and the accuracy expressed as the sum of quadratic residues (*SQR*).

Kinetic model	**Heating rate, β (°C/min)**	**Mn_2O_3 to Mn_3O_4 (reaction R4)**			**Mn_3O_4 to MnO (reaction R5)**		
		logA	***E* (kJ/mol)**	***SQR***	***logA***	***E* (kJ/mol)**	***SQR***
F_1	**2**	10.75	269.44	0.50	12.04	485.39	6.20
	5	10.35	261.87	0.40	11.86	480.17	2.42
	10	10.28	261.20	0.53	12.98	517.22	0.09
	20	10.06	256.57	0.31	13.16	522.59	0.11
R_3	**2**	8.39	235.15	0.41	9.28	417.83	10.16
	5	8.40	240.01	0.67	9.33	417.90	4.13
	10	7.98	226.40	0.29	10.97	469.13	0.20
	20	7.67	219.28	0.29	11.78	492.42	0.07
D_1	**2**	15.06	362.01	2.68	19.53	733.18	20.39
	5	15.13	363.20	2.79	15.90	624.98	11.69
	10	14.92	364.01	1.59	20.62	781.39	1.12
	20	14.65	360.56	1.22	24.29	905.04	0.02

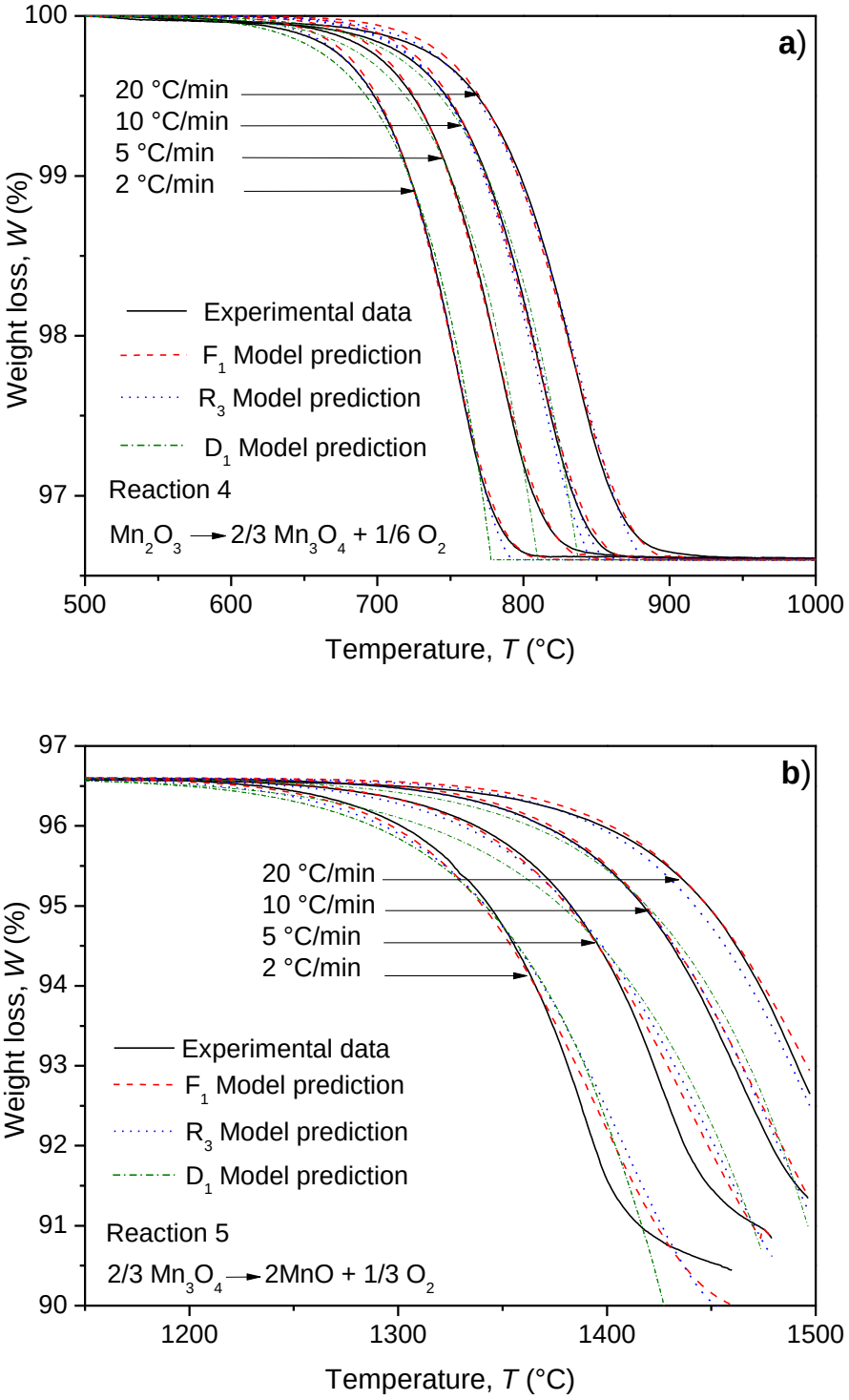

Figure 4. Comparison between the experimental TGA results and calculated data using F_1, R_3 and D_1 fitting models, a) reaction R4, and b) reaction R5.

Three different models with different mechanistic assumptions like F_1, R_3 and D_1 fit quite well the experimental data. The best fit was obtained for the first-order model, F_1, in which the reaction rate is proportional to the remaining fraction of reactant. The contracting volume model, R_3, reproduced also quiet well the results, specially for reaction R4. This model assumes that nucleation occurs rapidly on the surface of the solid, reducing consequently the volume of the original solid particle. Finally, the one-dimension diffusion model, D_1, is the third fitting model in terms of minimum values of SQR. In that model, the mobility of the constituents of the system is controlling the overall rate and the conversion fraction is directly proportional to product layer thickness [9]. However, the three models lead to significant differences in the values of activation energies and to differences in several orders of magnitud in the values of the pre-exponential factors. Moreover, for a fixed model, the values estimated for *E* and *A* are significantly different depending on the experimental heating rate. Thus, for the first order kinetic model, F_1, the best fitting model by far of all the tested, values of *logA* and *E* are ranging from 10.06 to 10.75 and 256.57 to 269.44 kJ/mol, respectively, depending on the heating rate. Opfermann [7] showed that virtually any model could fit an experimental TGA experiment changing the duplet *E* and *A*. This is due to the strong correlation existing between both kinetic parameters, that means that very similar fitting can be obtained for very different values of *E* and *A*. This relationship between *logA* and *E* has been widely reported in literature in many areas of chemistry, especially in heterogeneous catalysis. This phenomena, the Kinetic Compensation Effect (*KCE*) occurs when there is a linear relationship between *logA* and *E* for a family of related chemical processes [10]. However, the origin of *KCE* it is not clear, since it could have either physical significance or be the result of a purely mathematical origin for each particular case [11]. The representation of *logA vs. E* for the best fitting models is shown in Figure 5. It is clearly evident that all the data fit well with a linear regression, being the slope very similar for the two models (an average of 0.035 with an estandard deviation of 0.004). Thus, the *KCE* seems to be involved in the obtained results, either from physical or chemical reasons or mathematical errors. Nevertheless, from a theoretical viewpoint, these results are not acceptable, as the activation energy should be an intrinsic parameter of the process, independent of the kinetic model equation and the heating rate. In fact, several authors have proposed that the kinetic parameters lose their relevance in heterogeneous reactions in solid state, because the concepts of "order of reaction" and "concentration" are not applicable [12]. Thus, the parameters of the *KCE*, slope and interception in the linear regression, can be used as more realistic kinetic parameters describing the reactions. However, *E* and *logA* are still widely accepted kinetic

parameters for heterogeneous reactions in solid state. For that reason, a different approach was proposed in order to calculate these parameters avoiding the *KCE*. Thus, the model fitting previously described was carried out simultaneously to several experiments performed under different heating rates, assuming that the values of E and A are independent of β.

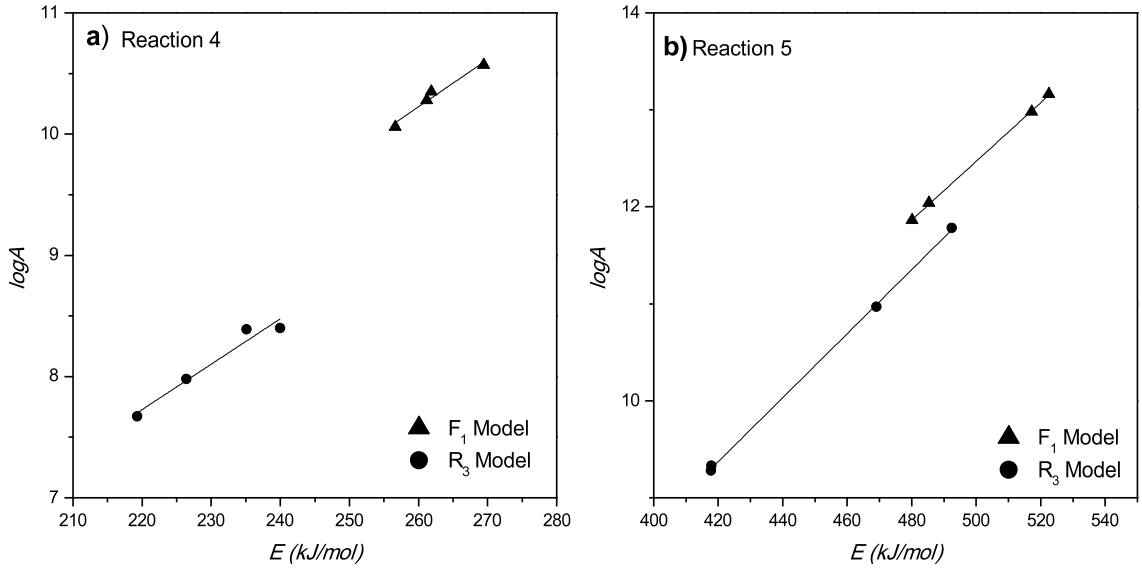

Figure 5. Linear relationship between *logA* and *E* obtained for the different heating rates and using the best fitting models shown previously, for a) Reaction 4 and b) Reaction 5.

3.2.2. Model fitting by simultaneously multivariate non-linear regression

Simultaneous fitting of TGA curves obtained under different heating rates allows the calculation of unique values of the Arrhenius parameters for a specific kinetic model. From all the 19 tested kinetic models, again the best fitting is obtained with F_1 and R_3 models. Figure 6 shows that a good agreement between the experimental data and the prediction of the model is achieved in both cases, whereas calculated values of *E* and *logA* are presented in Table 3 (those models with SQR values higher than 1000 have been removed from the table, due to their high error reproducing the experimental data). Nevertheless, the values estimated for the activation energy and the pre-exponential factor obtained with each model show a significant disparity. For that reason, a model free determination of the activation energy directly from the experimental data would be neccesary to estimate the value of *E* with increased physical significance.

Table 3. Kinetic parameters calculated for different kinetic models by simultaneous fitting of the TGA curves obtained under four different heating rates. The accuracy is expressed as the sum of quadratic residues (*SQR*).

Kinetic model	**Mn_2O_3 to Mn_3O_4 (Reaction R4)**			**Mn_3O_4 to MnO (Reaction R5)**		
	logA	***E* (kJ/mol)**	***SQR***	***logA***	***E* (kJ/mol)**	***SQR***
F_0	8.11	222.39	25.78	6.32	315.72	826.68
F_1	***10.03***	***255.87***	***2.29***	***11.82***	***478.76***	***40.48***
$F_{1.5}$	11.47	287.45	14.61	13.00	522.72	55.17
F_2	13.72	323.40	36.69	14.84	568.52	108.90
A_2	7.73	210.32	61.86	9.47	402.33	351.58
A_3	7.33	202.04	610.50	9.89	414.48	770.26
R_2	8.98	243.48	6.31	10.47	448.87	99.55
R_3	***8.75***	***241.62***	***2.92***	***11.06***	***471.91***	***74.65***
P_2	7.56	208.81	138.49	8.57	377.00	738.04
D_1	13.60	335.04	30.13	14.72	587.65	275.33
D_2	13.19	330.62	32.77	16.62	653.30	250.04
D_3	15.25	381.51	46.03	18.31	724.09	285.19
D_4	14.34	363.40	41.59	16.79	678.08	257.57
D_6	9.86	283.26	19.24	12.31	544.47	230.89

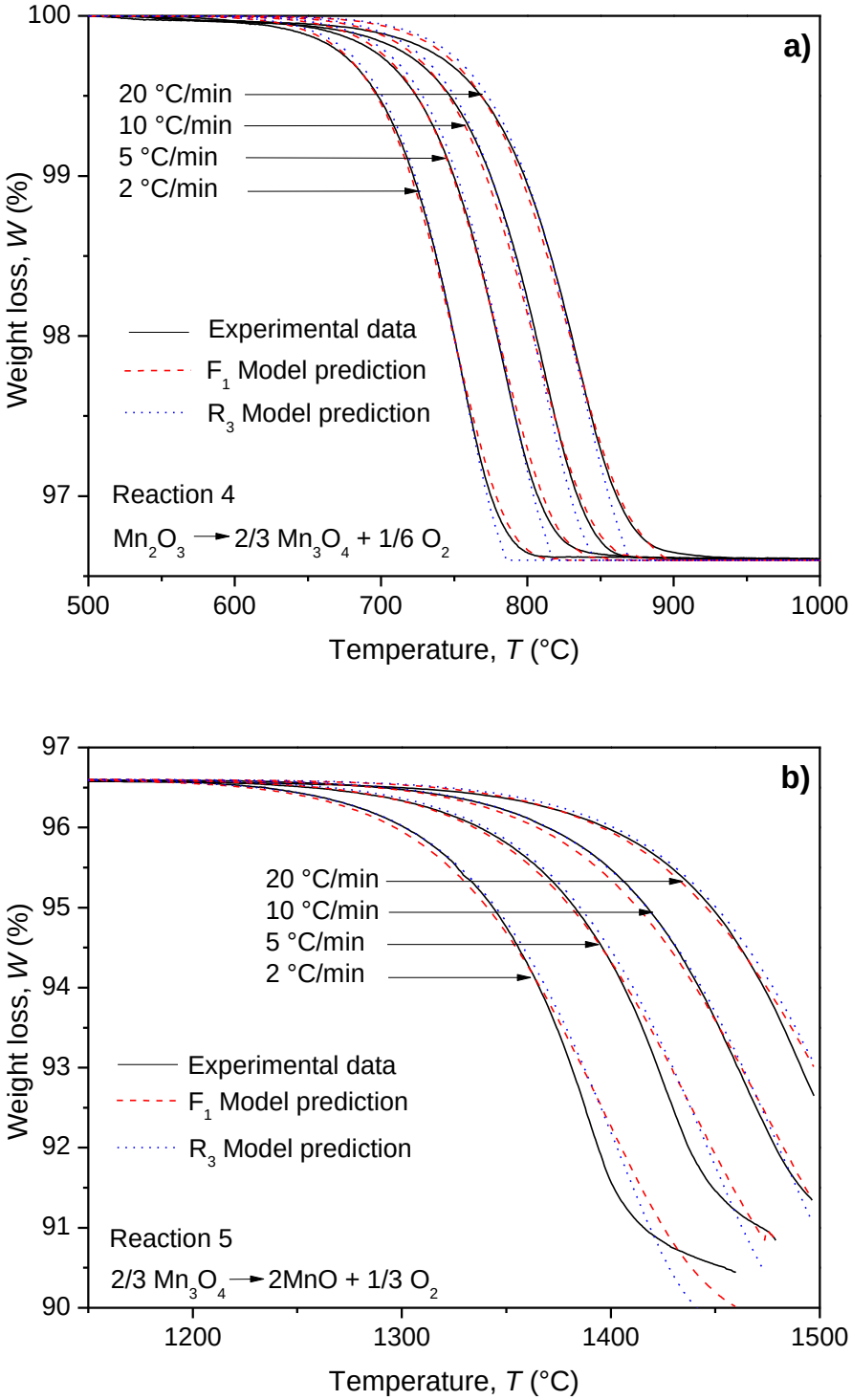

Figure 6. TGA experimental data at different heating ramps and predictions with F_1 and R_3 models, a) Reaction R4, and b) Reaction R5.

3.2.3. Isoconversional methods

Isoconversional methods allow the calculation of values for activation energies independent of the kinetic model. Different values of the activation energy can be estimated for each value of α [5, 8], being the dependence $E(\alpha)$ characteristic of the elementary processes occurring in the system. For that reason, when an isoconversional method is applied to multistep reactions and it reveals dependence of the activation energy on conversion, the shape of this dependence is indicative of the reaction mechanism [13]. Those methods have been widely applied in literature to obtain the thermal decomposition kinetics of polymers [14-16] or the dehydration kinetics of solids [17, 18]. Among the different isoconversional procedures reported in the literature, Ozawa [19] and Friedman [20] methods have been proposed for the calculation of activation energies of solid reactions at high temperatures.

a) Estimation of E by the Ozawa method

The isoconversional method proposed by Ozawa uses an approximation of Eq.3 in its integrated form (Eq.4), under the assumptions that E and A are independent of T:

$$\int \frac{d\alpha}{f(\alpha)} = \frac{A}{\beta}\int \exp\left(\frac{-E}{RT}\right)dT \qquad \text{(Eq.4)}$$

According to Doyle approximation [21], the right side of the Eq.4 can be written as a function of (E/RT), p, following the Eq.5 which can be approximated to Eq.6 if the condition $E/RT>20$ is fulfilled.

$$\int exp\left(\frac{-E}{RT}\right)dT = \frac{E}{R}\,p\left(\frac{E}{RT}\right) \qquad \text{(Eq.5)}$$

$$log\left[\,p\left(\frac{E}{RT}\right)\right] = -2.315 - 0.4567\frac{E}{RT} \qquad \text{(Eq.6)}$$

For a given value of α, the left side of Eq.4 is a constant independent of the heating rate. Thus, each value of the conversion could be obtained at different duplets β-T, which is

mathematically expressed by the Eq.7. Linear relationships expressed in Eq.8 can be derived from Eq.7 in combination with Eq.6.

$$\frac{AE}{\beta_1 R}\, p\left(\frac{E}{RT_1}\right) = \frac{AE}{\beta_2 R}\, p\left(\frac{E}{RT_2}\right) = \ldots \qquad \text{(Eq.7)}$$

$$-log\ \beta_1 - 0.4567\frac{E}{RT_1} = -log\ \beta_2 - 0.4567\frac{E}{RT_2} = \ldots \qquad \text{(Eq.8)}$$

Thus, for a fixed value of α, the activation energy as a function of α can be obtained from the slope of the plot logβ vs. 1/T (Eq.9).

$$\log\beta = \text{Constant value} - 0.456\frac{E}{RT} \qquad \text{(Eq.9)}$$

In this work, the Eq.9 was calculated for incremental values of α of 0.005, ranging from 0 to 1 in the case of the reaction R4, and 0 to 0.55 in the case of the reaction R5. Figure 7 shows some examples of the performed linear regression of the data at several different conversions. Although several authors have claimed that linearity of logβ vs. 1/T is not always achieved [22], in this case an excellent linear fit was obtained for all the values of α, with good correlation coefficients close to 1.0 in all cases, and for both reaction steps. Figure 8 shows the values calculated for E at incremental values of 0.005 for α.

In both cases (reactions R4 and R5), the activation energy can be considered to be not dependent on α except for low values of conversion (below 10 %). The slightly higher values of apparent E at the beginning of the reaction suggest the possible contribution to the global process of additional elementary steps to the chemical reaction (i.e. mass diffusion, [5]). However, for practical purposes, a constant value of the apparent activation energy can be assumed for the whole range of conversions. The mean values of E together with the standard deviation estimated from all the computed data calculated at different values of α are summarized in Table 4. As it has been mentioned previously, the value of activation energy

for reaction R5 has been estimated for conversions below 0.55 to ensure the statistical significance of regression slopes calculated with at least four heating rates data.

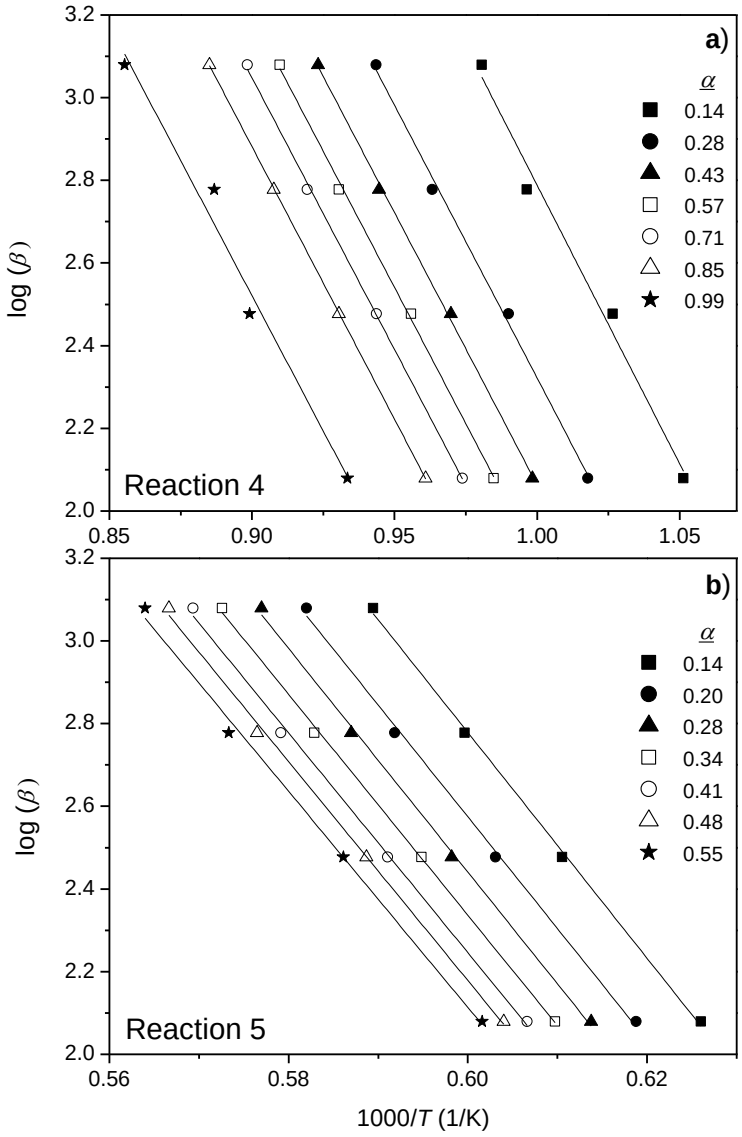

Figure 7. Calculation of *E* through the Ozawa method, a) reaction R4, and b) reaction R5.

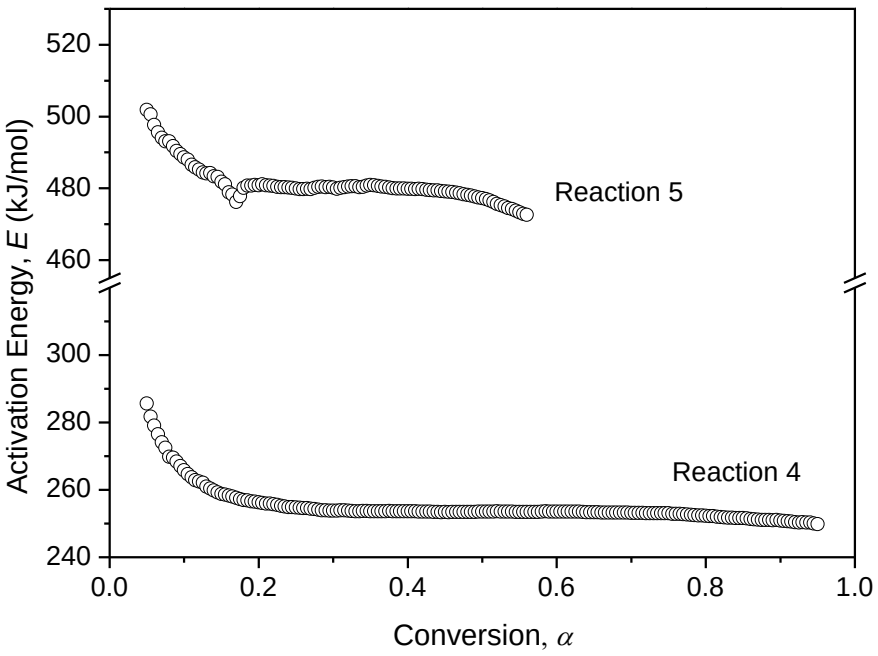

Figure 8. Influence of α in the activation energy calculated with the Ozawa method.

b). Estimation of E by the Friedman method

The Friedman method is based in the linearization of the derivative Eq.3, particularized for a value of α, as can be seen in Eq.10:

$$\ln\left[\beta\frac{d\alpha}{dT}\right] = \ln\left[-Af(\alpha)\right] - \frac{E}{RT} \qquad \text{(Eq.10)}$$

In that case, the activation energy for a fixed value of α can be obtained from the slope of the plot $\ln[\beta(d\alpha/dT)]$ vs. $1/T$.

Application of Friedman equation involves the preliminary calculation of the numerical derivative of the TGA curves in order to obtain $\ln[\beta(d\alpha/dT)]$ at fixed values of α. All the mathematical procedure was performed at incremental values of α of 0.005. As shown in

Figure 9 a good linear fit with correlation coefficients close to 1.0 can be obtained in all cases. Figure 10 depicts the dependence of calculated E with α for both reactions. In contrast with the results of the Ozawa method, in this case an almost constant value of the activation energy is obtained for both reactions, not indicating changes in the controlling phenomena of the global process even for low conversions. However, as a result of the numerical error of the computation of the $d\alpha/dT$ data, the standard deviation of the results is increased in comparison with results calculated by Ozawa method, as it can be seen in the mean values reported in Table 4.

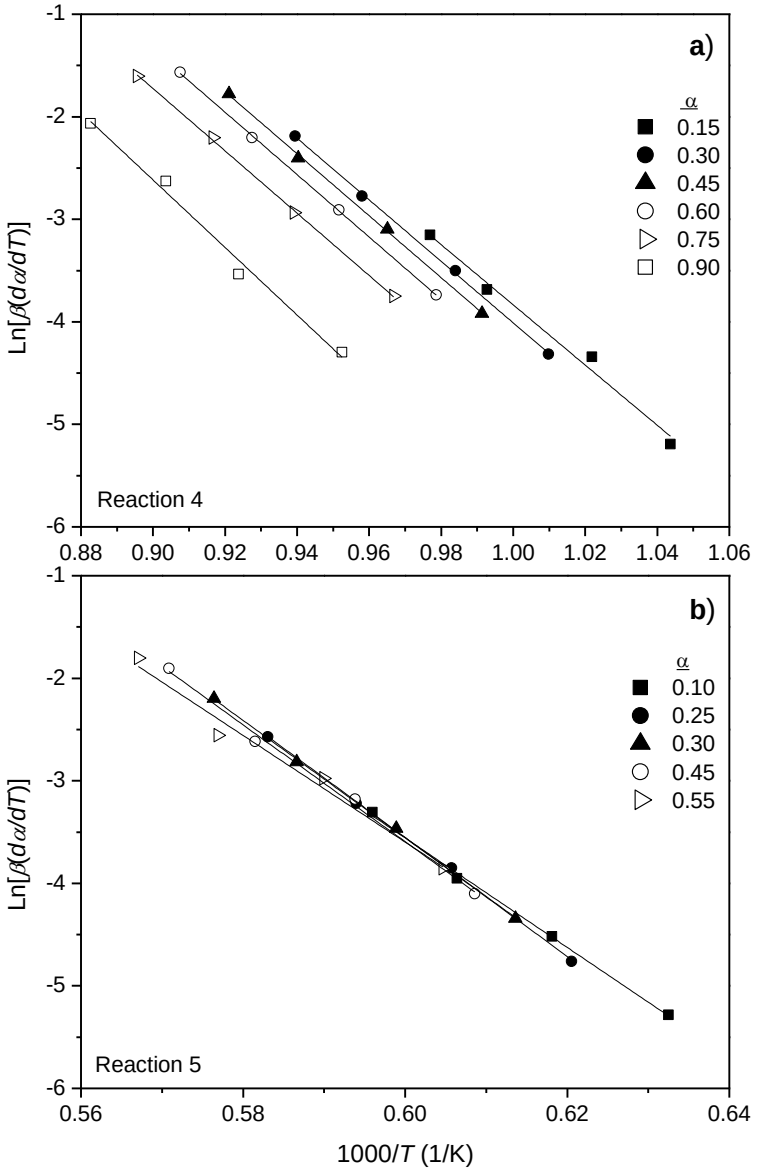

Figure 9. Calculation of E through the Friedman method, a) reaction R4, and b) reaction R5.

Table 4. Mean values of activation energy, *E*, calculated by Ozawa and Friedman methods.

	E_{OZAWA} (kJ/mol)	$E_{FRIEDMAN}$ (kJ/mol)
Reaction R4	254.14 ± 2.56	246.27 ±3.48
Reaction R5	479.76 ± 2.85	465.50 ± 20.5

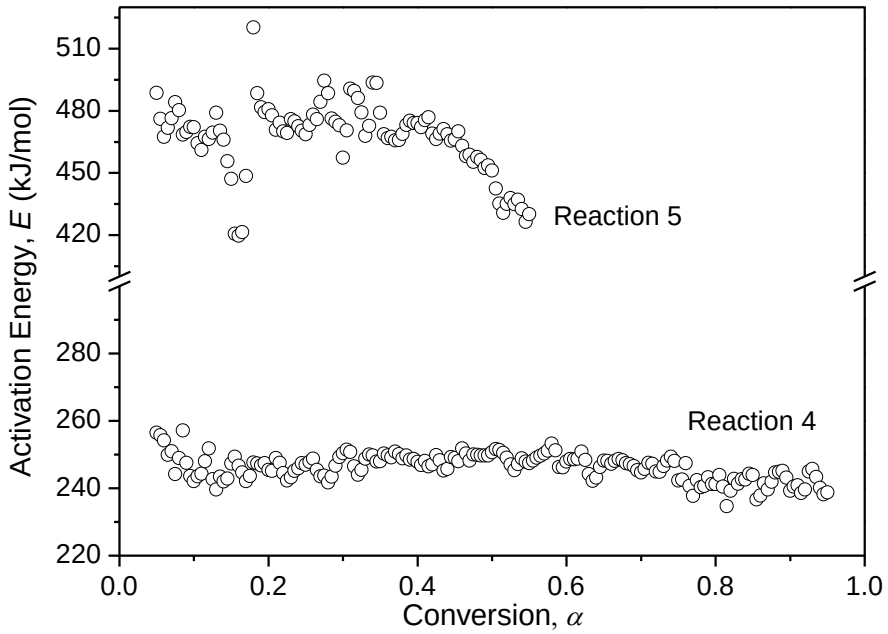

Figure 10. Influence of α in the activation energy calculated with the Friedman method.

3.3.3. Determination of the best kinetic model and calculation of the pre-exponential factor

The activation energies calculated by Ozawa or Friedman methods are not dependent of any kinetic equation. However, for the calculation of the pre-exponential factor both methods require the selection of a kinetic equation, following some numerical approximations and graphical calculations to obtain the average value of *logA*. For example, the Ozawa method requires the previous plot of the master thermogravimetric curve, independent of the heating rate, followed by the calculation of that curve for each kinetic model under study. From the difference between both graphical plots, *logA* can be inferred [19].

In contrast, in this work we propose that once those good values for the apparent activation energy have been estimated, the best values for the pre-exponential factor can be obtained by using a multivariate nonlinear regression method to fit simultaneously the data of all the experiments carried out with different heating rates. The procedure is similar to that previously described for the direct model fitting method, but in this case fixed values of *E* are used. In Figures 11 to 12 the comparison between the experimental TGA data obtained in the thermobalance and the predictive curves obtained with different kinetic models is shown. Those data have been obtained after previous optimization of the values of *logA* for reaction R4 and R5, obtaining the maximum accuracy for each model at fixed values of activation energy. Although diffusional models were proposed in Table 1 as possible kinetic models for reactions R4 and R5, accurate predictive values were not obtained using the activation energies calculated by the isoconversional methods. In this way, A_2 model was also not useful for prediction of reaction R5. For that reason, those models do not appear in Figures 11 and 12 (obtained with the activation energy calculated by the Ozawa method) nor Figures 13 and 14 (obtained with the activation energy calculated by the Friedman method).

Starting with the analysis of the models calculated with the activation energy from Ozawa (Figures 11 and 12), F_0 model predicts a narrower interval of temperatures for reaction R4, especially for the experiment at 2 ºC/min. Additionally, reaction R5 should be finished at 1425 ºC using that heating rate. $F_{1.5}$ and F_2 models underestimate the reaction progress, predicting higher temperatures to obtain the same weight loss than that obtained in the experiments in the thermobalance.

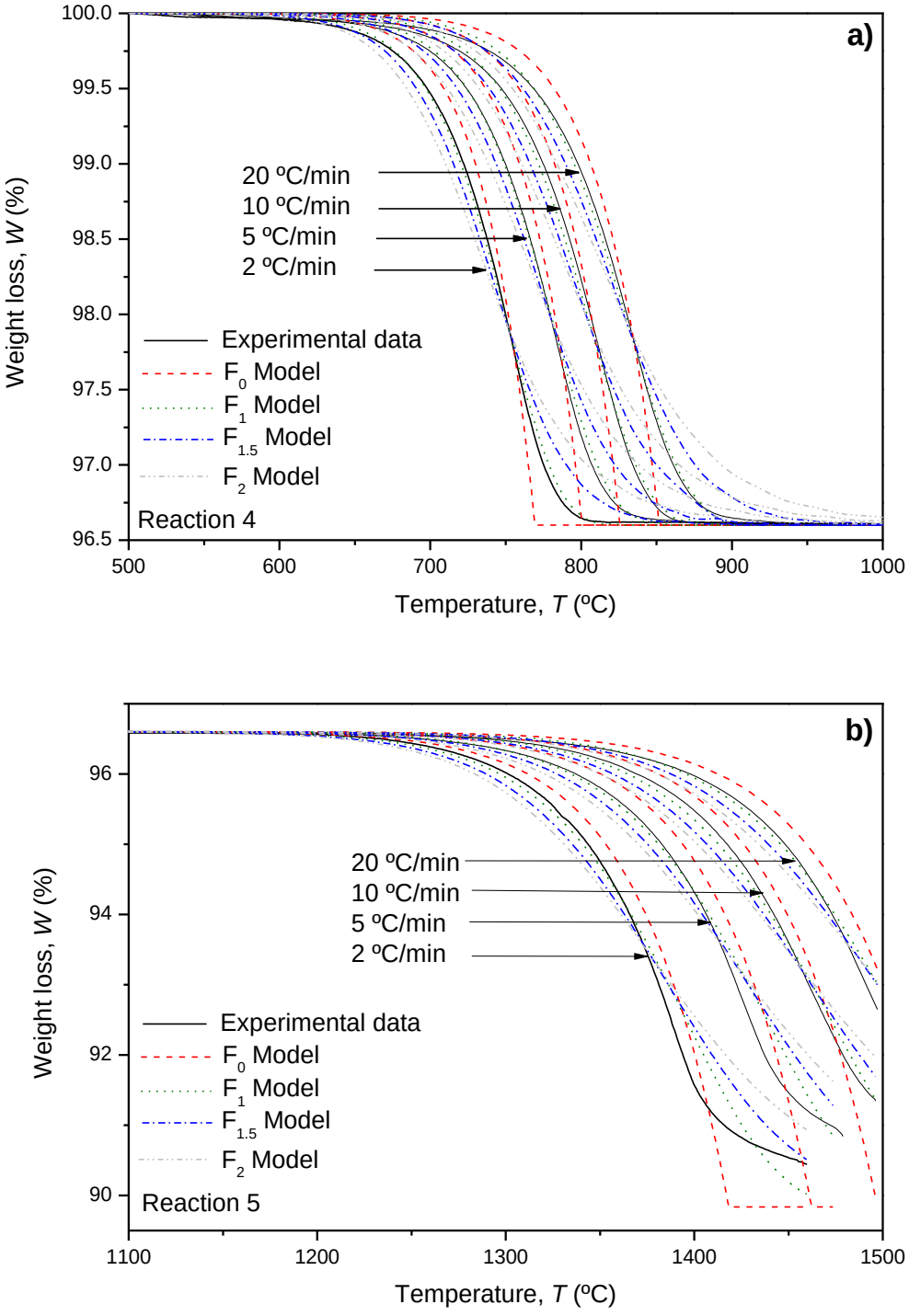

Figure 11. TGA experimental data at different heating ramps and predictions with kinetic-order model at fixed values of activation energy obtained with the Ozawa method. a) Reaction R4, E=254.14 kJ/mol, and b) Reaction R5, E=479.76 kJ/mol.

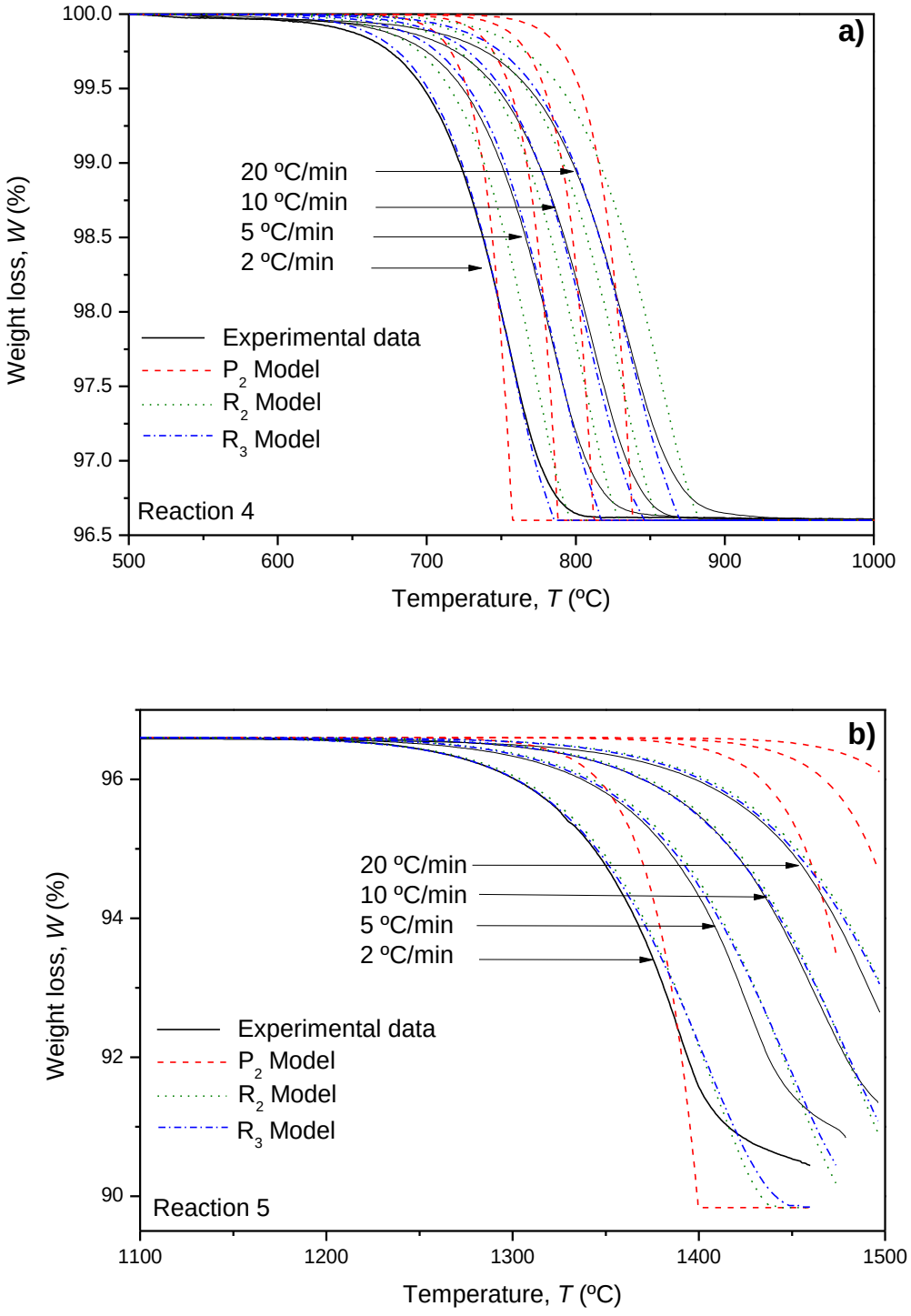

Figure 12. TGA experimental data at different heating ramps and predictions with contraction and nucleation models at fixed values of activation energy obtained with the Ozawa method. a) Reaction R4, E=254.14 kJ/mol, and b) Reaction R5, E=479.76 kJ/mol.

P_2 model fails by far the prediction of the experimental values of weight loss obtained in the thermobalance, especially for reaction R5. On the other hand, R_2 predicts higher temperatures for the values of weight loss than that obtained experimentally for reaction R4.

The same models but using the values of activation energy obtained by the Friedman equation were also evaluated. In that case, the behavior of the model curves are similar than that obtained previously with the Ozawa value of *E*. Nevertheless, differences respect to the experimental curves seems to be higher in this case (Figures 13 and 14).

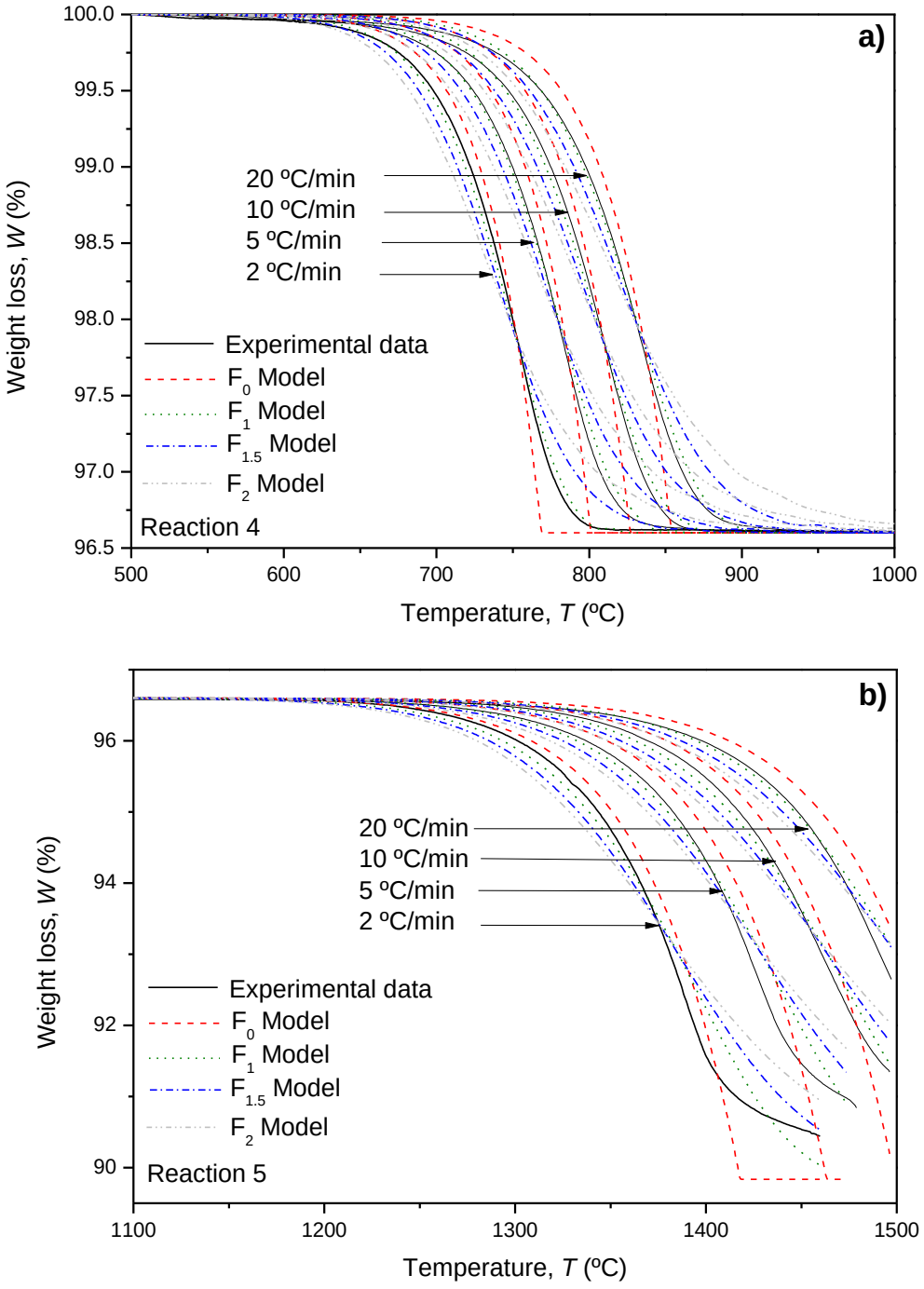

Figure 13. TGA experimental data at different heating ramps and predictions with kinetic-order model at fixed values of activation energy obtained with the Friedman equation. a) Reaction R4, E=246.27 kJ/mol, and b) Reaction R5, E=465.52 kJ/mol.

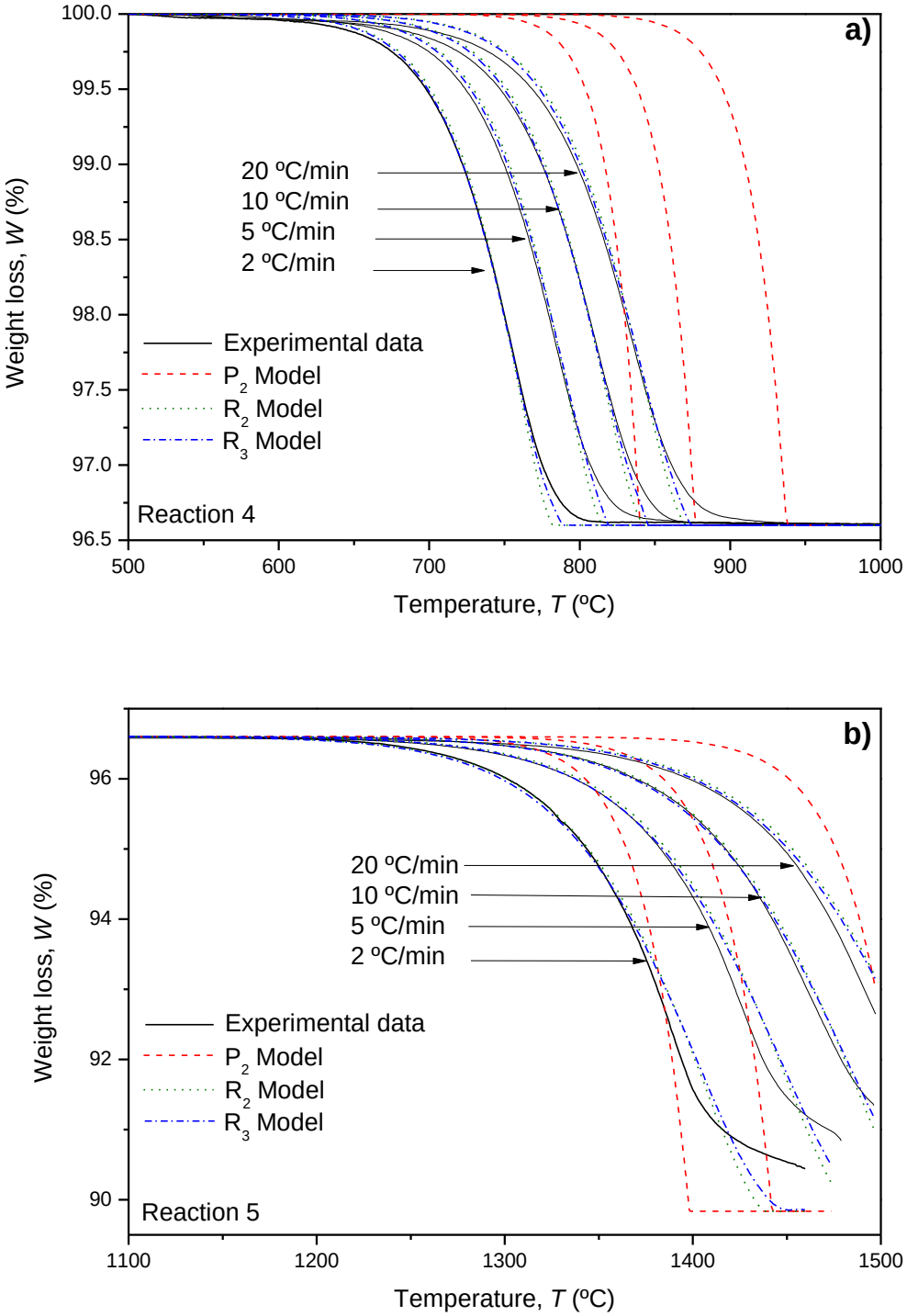

Figure 14. TGA experimental data at different heating ramps and predictions with contraction and nucleation models at fixed values of activation energy obtained with the Friedman equation. a) Reaction R4, E=246.27 kJ/mol, and b) Reaction R5, E=465.52 kJ/mol.

Once again, from all the different kinetic models, models F_1 and R_3 lead to the best fitting results, especially with E values estimated by Ozawa method. Table 5 summarizes the results obtained for the pre-exponential factor together with the corresponding fitting error. It is clearly evident from Figures 10-13 and Table 5 that reaction R4 is really well described by the kinetic parameters obtained in this work. On the other hand, the predictive data for reaction R5 obtained with the best fitting models (F_1 and R_3) show a considerable error especially at high temperatures (T>1350 ºC) and consequently at high weight loss or extent of that reaction, α. A plausible explanation could be that all the calculations have been done for values of α in the range of 0-0.55 for reaction R5, which could make unsteady predictions outside that range. Additionally, an average value of the activation energy, *E*, has been used for the determination of *logA* and evaluate the accuracy of the kinetic model. However, Figures 7 and 9 show a slight influence of the conversion in the activation energy at values of α higher than 0.45. This fact could be indicative of other predominant elementary step in the process, being necessary to introduce two different kinetic models describing reaction R5, one for α in the range of 0-0.45 and another kinetic model for higher values of conversion. Nevertheless, limitation in the number of points obtained in experiments performed at heating rates of 10 and especially 20 ºC/min makes not possible the evaluation of that second range of values of α at this moment. Consequently the kinetic parameters calculated for reaction R5 should only be considered for conversion values below 55%, and extrapolation to higher conversions and temperatures should previously validated by additional experimental data. In any case, this work confirms that the first step of the Mn_2O_3/MnO thermochemical cycle can be carried out at much lower temperatures that the theoretical temperatures estimated from the thermodynamic equilibrium [23] and that the kinetics of the process allow it to be conducted at reasonable values of the reaction rate.

Table 5. Kinetic parameters calculated with sequential isoconversional and multivariate nonlinear regression method. Fitting error expressed as the sum of quadratic residuals (*SQR*).

Reaction R4				
Kinetic Model	**Ozawa** E = 254.14 kJ/mol		**Friedman** E = 246.27 kJ/mol	
	Log *A* (min^{-1})	***SQR***	**Log *A*** (min^{-1})	***SQR***
F_1	9.94	2.31	9.53	3.04
R_3	9.40	14.72	8.99	3.17
Reaction R5				
	Ozawa *E* = 479.76 kJ/mol		**Friedman** E = 465.52 kJ/mol	
Model	**Log *A*** (min^{-1})	***SQR***	**Log *A*** (min^{-1})	***SQR***
F_1	11.85	39.58	11.40	41.35
R_3	11.31	72.25	10.86	69.73

4. Conclusions

The combination of isoconversional methods for the estimation of realistic activation energy values and a multivariate nonlinear regression procedure for the determination of the best kinetic model and pre-exponential factor has allowed the calculation of the kinetic parameters of the first step of the Mn_2O_3/MnO thermochemical cycle for solar H_2 production. The process takes place through two sequential reactions following a first order kinetic model with activation energies of 254.14 and 479.76 kJ/mol and pre-exponential factors of 8.71×10^9 and 7.08×10^{11} min^{-1}, respectively.

Acknowledgement

The authors wish to thank “Comunidad de Madrid” and “European Social Fund” for its financial support to the SOLGEMAC Project through the Program of Activities between Research Groups (S2009/ENE-1617). Financial support of Ministerio de Ciencia e Innovación of Spain (Plan Nacional de Investigación Científica, Desarrollo e Innovación

Tecnológica 2008-20) and Fondo Europeo de Desarrollo Regional (FEDER) through the program PSE-H2RENOV SP4-HYTOWER (PSE-120000-2009-3) is also gratefully acknowledged. C. Herradón also thanks Universidad Rey Juan Carlos for its PhD grant.

References

[1] Pregger T, Graf D, Krewitt W, Sattler C, Roeb M, Möller S. Prospects of solar thermal hydrogen production processes. International Journal of Hydrogen Energy 2009; 34:4256-4267.

[2] Perkins C, Weimer AW. Likely near-term solar-thermal water splitting technologies. International Journal of Hydrogen Energy 2004; 29:1587-1599.

[3] Sturzenegger M, Nüesch P. Efficiency analysis for a manganese-oxide-based thermochemical cycle. Energy 1999; 24:959-970.

[4] Francis TM, Lichty PR, Weimer AW. Manganese oxide dissociation kinetics for the Mn_2O_3 thermochemical water-splitting cycle. Part I: Experimental. Chemical Engineering Science 2010; 65:3709-3717.

[5] Vyazovkin S, Wight CA. Kinetics in solids. Annual Review of Physical Chemistry 1997; 48: 125-149.

[6] Noisong P, Danvirutai C. Kinetics and mechanism of thermal dehydration of $KMnPO_4 \cdot H_2O$ in a nitrogen atmosphere. Industrial and Engineering Chemistry Research 2010; 49: 3146-3151.

[7] Opfermann J. Kinetic analysis using multivariate non-linear regression. Journal of Thermal Analysis and Calorimetry 2000; 60: 641-658.

[8] Czarnecki J, Sestak J. Practical thermogravimetry. Journal of Thermal Analysis and Calorimetry 2000; 60: 759-778.

[9] Khawam A, Flanagan DR. Solid-State Kinetic Models: Basics and Mathematical Fundamentals. Journal of Physical Chemistry B 2006; 110: 17315-17328.

[10] Zsako J, The kinetic compensation effect. Journal of Thermal Analysis 1976; 9: 101-108.

[11] Barrie PJ, The mathematical origins of the kinetic compensation effect: 2. the effect of systematic errors. Physical Chemistry Chemical Physics 2012; 14: 327-336.

[12] Liu N, Zong R, Shu L, Zhou, Fan W, Kinetic Compensation Effect in Thermal Decomposition of Cellulosic Materials in Air Atmosphere. Journal of Applied Polymer Science 2002; 8: 135-141.

[13] Vyazovkin S, Dollimore D. Linear and Nonlinear Procedures in Isoconversional Computations of the Activation Energy of Nonisothermal Reactions in Solids. Journal of Chemical Information and Computer Sciences 1996; 36: 42-45.

[14] Yang MH. On the thermal degradation of poly(styrene sulfone)s III. Thermal degradation of poly(acrylamide sulfone)s. Polymer Degradation and Stability 2000; 68: 451-458.

[15] Lee JY, Shim MJ, Kim SW. Thermal decomposition kinetics of an epoxy resin with rubber-modified curing agent. Journal of Applied polymer Science 2001; 8: 479-485.

[16] Wang SX, Tan ZC, Li YS, Sun LX, Li Y. A kinetic analysis of thermal decomposition of polyaniline/ZrO_2 composite. Journal of Thermal Analysis and Calorimetry 2008; 92: 483-487.

[17] Kanungo SB, Mishra SK. Kinetics of thermal dehydration and decomposition of Fe(III) chloride hydrate ($FeCl_3 \cdot xH_2O$). Journal of Thermal Analysis 1997; 48: 385-401.

[18] Straszko J, Olszak-Humienik M, Mozejko J. The kinetic parameters of thermal decomposition hydrated iron sulphate. Journal of Thermal Analysis 1997; 48: 1415-1422.

[19] Ozawa T. A new method of analyzing thermogravimetric data. Bulletin of the Chemical Society of Japan 1965; 38: 1881-1886.

[20] Friedman HL. Kinetics of thermal degradation of charm-forming plastics from thermogravimetry. Journal of Polymer Science Part C. Polymer Symposia 1964; 6: 183-195.

[21] Doyle CD. Kinetic analysis of thermogravimetric data. Journal of Applied Polymer Science 1961; 5: 285-292.

[22] Vyazovkin S. Advanced isoconversional method. Journal of Thermal Analysis and Calorimetry 1997; 49: 1493-1499.

[23] Marugán J, Botas JA, Martín M, Molina R, Herradón C. Study of the first step of the Mn_2O_3/MnO thermochemical cycle for solar hydrogen production. International Journal of Hydrogen Energy 2012; 37: 7017-7025.